2-2013

Shear-induced detachment of biofilms from hollow fiber silicone membranes

Z. Huang
Birck Nanotechnology Center, Purdue University

E. S. McLamore
University of Florida

H. S. Chuang
Purdue University

W. Zhang
University of Arkansas - Fayetteville

Steven Wereley
Birck Nanotechnology Center, Purdue University, wereley@purdue.edu

See next page for additional authors

Huang, Z.; McLamore, E. S.; Chuang, H. S.; Zhang, W.; Wereley, Steven; Leon, J. L. C.; and Banks, M. K., "Shear-induced detachment of biofilms from hollow fiber silicone membranes" (2013). *Birck and NCN Publications.* Paper 1330.
http://dx.doi.org/10.1002/bit.24631

Authors
Z. Huang, E. S. McLamore, H. S. Chuang, W. Zhang, Steven Wereley, J. L. C. Leon, and M. K. Banks

ARTICLE

BIOTECHNOLOGY and BIOENGINEERING

Shear-Induced Detachment of Biofilms From Hollow Fiber Silicone Membranes

Z. Huang,[1,2,3] E.S. McLamore,[4] H.S. Chuang,[5] W. Zhang,[6] S. Wereley,[3,5] J.L.C. Leon,[4] M.K. Banks[1,2,3]

[1]School of Civil Engineering, Purdue University, 550 Stadium Mall Dr., West Lafayette, IN 47907; telephone: 765-494-2256; fax: (979) 845-6156; e-mail: k-banks@tamu.edu

[2]Bindley Bioscience Center, Physiological Sensing Facility, Purdue University, West Lafayette, IN

[3]Birck Nanotechnology Center, Purdue University, West Lafayette, IN

[4]Agricultural and Biological Engineering Department, University of Florida,Gainesville, FL

[5]Department of Mechanical Engineering, Purdue University, West Lafayette, IN

[6]Department of Civil Engineering, University of Arkansas, Fayetteville, AR

ABSTRACT: A suite of techniques was utilized to evaluate the correlation between biofilm physiology, fluid-induced shear stress, and detachment in hollow fiber membrane aerated bioreactors. Two monoculture species biofilms were grown on silicone fibers in a hollow fiber membrane aerated bioreactors (HfMBR) to assess detachment under laminar fluid flow conditions. Both physiology (biofilm thickness and roughness) and nutrient mass transport data indicated the presence of a steady state mature biofilm after 3 weeks of development. Surface shear stress proved to be an important parameter for predicting passive detachment for the two biofilms. The average shear stress at the surface of *Nitrosomonas europaea* biofilms (54.5 ± 3.2 mPa) was approximately 20% higher than for *Pseudomonas aeruginosa* biofilms (45.8 ± 7.7 mPa), resulting in higher biomass detachment. No significant difference in shear stress was measured between immature and mature biofilms of the same species. There was a significant difference in detached biomass for immature vs. mature biofilms in both species. However, there was no difference in detachment rate between the two species.

Biotechnol. Bioeng. 2013;110: 525–534.

KEYWORDS: detachment; momentum transport; biofilm; boundary layer; shear stress

Introduction

Biofilm physiology is a temporally and spatially dynamic process that depends on mass transport, hydrodynamics, stage of growth, and chemical/physical stressors such as chemical toxins or abrasion (Cole et al., 2004; Picioreanu et al., 1998; Stoodley et al., 2004, 2005; Wimpenny and Colasanti, 1997). Biofilms actively regulate morphological features (e.g., formation of streamers, microchannels, and mushroom bodies) through differentiation and expression of genes that directly control spatial organization of cells, and biofilm formation is often considered a stochastic process that is dependent on species type as well as growth conditions (Stoodley et al., 2002a, 2004).

Reactors engineered to support biofilm growth (i.e., attached growth reactors) have gained attention in the last few decades due to increased cell density, protection from physical/chemical stressors, and the ability to form stratified community physiology based on mass transfer of nutrients/byproducts. One of the major challenges with biofilm reactors is maximizing convective transport to the biofilm without causing detachment. Uncontrolled biofilm detachment causes a decrease in reactor processing efficiency, and can also lead to human pathogen exposure in downstream processors (Boles et al., 2005). Detailed studies are needed for understanding the detachment of biofilms from different types of engineered biofilm reactors that vary in geometry and operating conditions.

Biofilm detachment depends on temperature, nutrient availability, hydrodynamics, and presence of chemical toxins (Picioreanu et al., 2001; van Loosdrecht et al., 1995). Passive detachment is defined as detachment caused by external forces such as shear, erosion, sloughing, abrasion, and predator grazing; while active detachment

Correspondence to: M.K. Banks

Additional supporting information may be found in the online version of this article.
Received 29 February 2012; Revision received 23 July 2012; Accepted 26 July 2012
Accepted manuscript online 7 August 2012;
Article first published online 22 August 2012 in Wiley Online Library (http://onlinelibrary.wiley.com/doi/10.1002/bit.24631/abstract)
DOI 10.1002/bit.24631

refers to internally driven mechanisms (Picioreanu et al., 2001; Stoodley et al., 2001). Flow conditions and the geometry of the media are major driving forces for detachment. Biofilms formed under laminar flow are less dense than biofilms formed under turbulent conditions, and have been shown to detach with relative ease (Chen et al., 1998; Ohashi and Harada, 1994). Biofilms grown on flat surfaces form interconnected cell clusters, while biofilms on concave and convex tubular surfaces tend to form continuous biofilms with a relatively uniform cell distribution (Wijeyekoon et al., 2000). While these fundamental observations can be used to predict basic biofilm behavior, to date few detailed studies have been conducted for biofilms grown on concave/convex surfaces. Experiments describing biofilm formation on concave surfaces such as silicone membrane fibers are critical to understanding reactor startup and efficiency of HfMBR, as the biofilm physiology is significantly different than traditional biofilm reactors.

Biofilms in HfMBR are immobilized on the exterior (convex) surface of hollow polydimethylsiloxane (PDMS) membranes. For aerobic HfMBR, oxygen diffuses across the semi-permeable PDMS fiber wall to the biofilm from the attachment site, and also from the bulk liquid phase into the biofilm (known as counter-diffusion) (Wang et al., 2009). HfMBR have demonstrated improved gas transfer, high areal conversion rates (see Rector et al., 2006 for description of areal conversion rates), low energy demand, low maintenance, and reduced volatile stripping (Casey et al., 1999, 2000; Cote et al., 1989) relative to traditional co-diffusion biofilm reactors. HfMBRs are widely used for a number of applications, including nitrification (Suzuki et al., 2000), acetonitrile degradation (Li et al., 2009), simultaneous organic carbon removal and nitrification (Yamagiwa et al., 1998), single stage nitrification and denitrification (Hibiya et al., 2003; Terada et al., 2003), treatment of raw sewage (Pankhania et al., 1994), urine treatment (Tansel et al., 2005, 2006), and sulfide removal (Sahinkaya et al., 2011).

Previous studies have evaluated the physiology of mature *Pseudomonas aeruginosa* and *Nitrosomonas europaea* biofilms on PDMS fibers (Jaroch et al., 2011; McLamore et al., 2009, 2010a). These monoculture HfMBR studies provided fundamental data describing metabolism and stress response under various operating conditions. However, to date no studies have investigated the detachment of these monoculture biofilms from PDMS fibers under conditions commonly used in wastewater processing.

This paper employs a suite of techniques to measure physiology, shear stress, and detachment rate for a chemolithoautotrophic (*N. europaea)* and a chemoorganoheterotorphic (*P. aeruginosa)* biofilm grown on hollow fiber membranes. Basic physiology (metabolic flux, roughness, thickness) was measured during biofilm development. Once biofilms achieve steady state conditions, detailed passive detachment studies were conducted using a range of fluid velocities in a constructed flow cell.

Materials and Methods

Biofilm Culture

P. aeruginosa (Schroeter) Migula (ATCC 27853) and *N. europaea* Winogradsky (ATCC 19718) were purchased from the American Type Culture Collection (Manassas, VA). All reactors were inoculated with 1mg/L of suspended monoculture bacteria. Biofilms were grown in autoclaved upflow hollow fiber membrane-aerated bioreactors (HfMBR) (McLamore et al., 2007). Non-porous PDMS (Silastic©) silicone membranes (Dow Corning Co., Midland, MI) were attached to reactor caps using threaded ferrules (Direct Industry, Sarasota, FL), which allowed individual fibers to be easily removed when needed. Filtered air was pumped through the membrane lumen at a transmembrane pressure of 10 kPa. *P. aeruginosa* was grown on glucose-enriched trypticase soy broth; 10 mM glucose and 10 mM Tris buffer (pH 7.4; Sigma–Aldrich, St. Louis, MO) according to McLamore et al. (2010a). *N. europaea* was grown in ATCC 2265 media (McLamore et al., 2009, 2010a).

HfMBRs effluent water quality was analyzed weekly, and steady state performance was based on the criteria outlined in McLamore et al. (2009). All reactors were located in a sterilized environmental growth chamber within a class 10 clean room. Reactor sampling procedures are described in McLamore et al. (2009, 2010a,b). Silicone membrane fibers (5 mm long each) were removed from reactors and attached to the constructed flow cell using the threaded ferrules to limit biofilm detachment during transfer.

Biofilm Thickness and Roughness

Biofilm thickness was measured using a high resolution Pulnix progressive scan camera (JAI, Inc., San Jose, CA) with an Optem 70XL zoomscope (Fairport, NY) and a National Instruments frame grabber (Austin, TX) with custom optical profiling software described in McLamore et al. (2010a,b). Briefly, the biofilm was focused at 7× magnification using a stepped motor platform (McLamore et al., 2009) attached to a vibration isolation table (Technical Manufacturing Corporation, Peabody, MA). The location of the biofilm surface relative to the fiber wall was recorded using a frame locator at ten locations along each biofilm. All measurements were collected at a standard position controlled by the stepped motor to ensure accuracy relative to the fiber wall. After measurement of the 5 mm long biofilm sample, the fiber was rotated in 30° increments using the threaded swivel ferrules in the flow cell. Average thickness was calculated using all values measured during rotation. Biofilm thickness was calculated by subtracting the average vertical position of the bare membrane from the position of the biofilm surface, and values averaged for three replicate biofilm samples.

Biofilm surface roughness was calculated using custom optical profiling software based on McLamore et al. (2010b).

Root mean square (RMS) values were calculated using Veeco software (RMS is the standard deviation of the Z values measured in contact mode) (Auerbach et al., 2000).

Flow Field Measurements

Flow visualization was conducted using a micro particle image velocimetry (μ-PIV) apparatus (Santiago et al., 1998). Briefly, 3 μm fluorescent particles (1% solid volume fraction, excitation: 542 nm, emission: 612 nm; Duke Scientific, Palo Alto, CA) were seeded in deionized water at a concentration of 6.7×108 particles/mL for the target fluid. A double-pulse Nd:YAG laser (Gemini15 120 mJ/pulse, New Wave Research, Portland OR) was used to produce high illumination for the flow plane. The illuminated plane in the targeted flow with particles was evaluated with a Sony high resolution camera (1,300 × 1,030 pixels, pixel size = 6.45 μm, 12 bit; Lavision, Ann Arbor, MI). A series of paired images between two distinct time intervals (Δt) were recorded from the illuminated plane. The images were then processed with Education Particle Image Velocimetry software (http://www.edpiv.com/) to determine the distance (Δx) particles travel during the time interval. The particle velocity was calculated using the spatially averaged cross-correlation algorithm in combination with median filtration, 9-point Gaussian peak detection, vector validation, and a smoothing algorithm.

The hydrodynamic boundary layer (HBL) thickness near biofilms was measured using μPIV. A syringe pump was used to control the flow rate (5, 10, and 15 mL/min) in the constructed flowcell for each experiment. All biofilm samples were taken from a single membrane fiber, and a new sample from the HfMBR was used for each experiment. Before each measurement, fluid was pumped for at least three hydraulic retention times to allow for flow stabilization. Clean, sterile membranes were used as a control for all measurements. The thickness of the HBL was defined as the location in the direction perpendicular to flow (y) where the measured velocity (u) was 99% of the free stream velocity (u_∞).

Calculation of Shear Stress and Dimensionless Parameters

The surface shear stress (τ_s; see Supplementary Fig. S1) was calculated using the linear portion of the velocity profile according to Equation (1), where μ is the viscosity of the solution and y is vertical distance from biofilm surface:

$$\tau_s = \mu \frac{\partial u}{\partial y} \tag{1}$$

For calculating the axial Reynolds number (Re), the flowcell was treated as an annular tube (Fig. S1; Equation 2); where D is the hydraulic diameter ($D = D_o - D_i$), D_o is the diameter of the flow cell, and D_i is the outer diameter of the silicone membrane (see Supplementary Fig. S1):

$$\mathrm{Re} = \frac{\rho u_\infty D}{\mu} \tag{2}$$

All measurements were performed in the geometric center of the flowcell where L/D (length to diameter ratio) was greater than 3 (L was the distance from the inlet to the measurement location). An L/D ratio greater than 3 ensures that fully developed flow exists, and minimizes entrance, stagnation, and exit effects (Higuchi et al., 2005).

Physiological Flux

Metabolic flux was measured using the self-referencing (SR) microsensor technique described in the literature for oxygen (McLamore et al., 2010a), ammonium (McLamore et al., 2009), and glucose (Jaroch et al., 2011). SR is a technique that directly monitors concentration gradients (ΔC) during oscillation of a microsensor by a constant distance (ΔX) at the surface of a biofilm. Flux values (J) were calculated using Fick's first law of diffusion ($J = -D\Delta C \Delta X^{-1}$). SR discretely corrects for signals produced by ambient drift and noise using phase sensitive detection (reviewed in detail by McLamore and Porterfield, 2011).

Physiological oxygen flux was measured using a SR optical oxygen sensor, which was constructed by immobilizing an oxygen-quenched fluorescent dye (platinum tetrakis pentafluoropheynl porphyrin) on the tip of a tapered optical fiber (5 μm tip diameter) (McLamore et al., 2010a). For *P. aeruginosa* biofilms, substrate (glucose) flux was measured using a nanomaterial-mediated glucose biosensor (McLamore et al., 2011) that was fabricated by entrapping glucose oxidase within a Nafion/carbon nanotube layer on the tip of a Pt/Ir wire. For *N. europaea* biofilms, substrate (NH_4^+) flux was measured using a microelectrode fabricated by immersing a Ag/AgCl wire in a tapered glass capillary containing electrolyte and a liquid membrane selective for NH_4^+ (McLamore et al., 2009). The diffusion coefficients used to calculate ammonium, glucose, and oxygen flux may be found in the literature (McLamore et al., 2009, 2010a, 2011).

Physiological flux was continuously monitored at five positions along the surface of 5 cm biofilm segments for 20 min unless otherwise indicated. All flux values represent averages of the arithmetic mean (at least 10 min of continuous recording) at five different positions ($n = 3$ replicates), and error bars for all physiological flux data represent the standard error of the arithmetic mean.

Measuring Biomass

Detached biomass was measured using either standard solids testing (EPA, 2010) or using a Beckman Multisizer 4

Coulter Counter (Beckman Coulter, Fullerton, CA). The lower limit of detection for standard solids testing (1.5 mg/L; EPA, 2001) does not allow small scale, rapid experiments to be conducted in constructed flowcells such as the device herein. Coulter counters are ideal for measuring biomass below 1.5 mg/L, although most coulter counters are not suitable for biomass concentrations above 1.5 mg/L due to blockage of the aperture. Therefore, the coulter counter method was used for short-term detachment studies, and standard solids testing was used for long-term studies.

For standard solids testing, crucibles were dried at 105°C overnight to remove any water, and then weighed. Triplicate liquid samples (5 mL) containing biomass were placed in the crucibles and dried at 105°C, cooled, and weighed again. Total solids content was (mg-solids/L) calculated using standard procedures. A blank sample containing DI water was analyzed for comparison. For measuring biomass concentrations below 1.5 mg/L, the techniques reported in Jaroch et al. (2011) were used.

For all coulter counter measurements, liquid effluent was collected in autoclaved bottles containing 5 mL of isotone solution (Beckman Coulter) and trypsinized using GIBCO EDTA/trypsin solution (Invitrogen, Carlsbad, CA) for 5 min. A Beckman Multisizer 4 Coulter Counter (Beckman Coulter) was used to measure the concentration of the detached biomass (consisting of particles 0.4 μm to 2 mm in size). Individual samples were each assessed nine times to collect an average biomass concentration. For all plots of detachment data, average values represent the average biomass concentration measured for three replicate samples (measured nine times each).

Biofilm Development and Detachment Studies

For time course studies of biofilm development, PDMS fibers were placed in the constructed flowcell and inoculated with 1 mg/L of monoculture cell suspensions. The transmembrane pressure was maintained at 10 kPa throughout all experiments. Biofilms were exposed to media as previously described, and liquid effluent was recirculated to maintain a mean stream velocity of 22 mm s^{-1} ($Re = 20$). For detailed studies of shear-induced detachment of mature biofilms, fiber samples with mature biofilms (5 cm in length) were transferred to the flow cell and exposed to a constant velocity for 20 min (see Fig. 5 for specific velocities in each experiment). Effluent samples were collected and analyzed for biomass using either standard solids testing or a coulter counter (see below for details). The coulter counter method was used unless the aperture blocked, in which case standard solids analysis was used to measure biomass.

The steady state behavior of biofilm thickness, roughness, and HBL thickness is similar to correlations observed for biofilms grown on inert media (Bishop et al., 1997) and flat sheets (Shanahan and Semmens, 2007). Detailed experiments investigating the effect of fluid shear on detachment in this study were measured between 2.9 and 46.8 mm s^{-1}, which represents a recycle ratio of 20–350 at the loading rates used in this study based on the transport model developed by Rector et al. (2006).

Statistical Analysis

Where indicated, statistical tests were used to test for significance; either analysis of variance (ANOVA) or student's *t*-test. For all tests, the significance level (α) was 0.05.

Results and Discussion

Biofilm Development

One week old *N. europaea* biofilms grown at $Re = 20$ ($u_\infty \approx 23$ mm s^{-1}) had a thickness of 13 ± 11 μm and a roughness of 60 ± 3 μm. One-week-old *P. aeruginosa* had a thickness of 10 ± 6 μm and a roughness of 18 ± 2 μm (Fig. 1, panels A and B). Biofilm thickness and roughness were not significantly different during the first week of growth ($P = 2.2 \times 10^{-3}$, $\alpha = 0.05$). After 3 weeks of growth at $Re = 20$, *N. europaea* and *P. aeruginosa* biofilms had an average thickness of 199 ± 12, and 25 ± 12 μm, respectively; and an average roughness of 82 ± 7, and 18 ± 8 μm, respectively. After 2 weeks, *N. europaea* and the *P. aeruginosa* thickness and roughness exhibited a stable value after 3 weeks that did not significantly change ($P = 1.1 \times 10^{-2}$, $\alpha = 0.05$), indicating steady state growth. However, the thickness and roughness of mature *N. europaea* was significantly larger than the mature *P. aeruginosa* biofilms. Following the lag in biofilm thickness during week 1, the change in thickness (during week 1–2) was calculated to estimate exponential growth rate. Based on this calculation, *N. europaea* growth rate (1.11 μm h^{-1}) was significantly higher than the *P. aeruginosa* growth rate (0.07 μm h^{-1}). These values are different from those reported by other researchers, as specific growth rates reported for planktonic *P. aeruginosa* (0.29 h^{-1}; Beyenal et al., 2003) are much higher than *N. europaea* (0.017–0.088 h^{-1}; Kindaichi et al., 2006; Prosser, 1989). However, the physiology of the growth conditions are significantly different (Stoodley et al., 2002a, 2004). To further investigate this observed pattern of growth between *N. europaea* and *P. aeruginosa* biofilms, substrate and oxygen flux were measured during development.

Oxygen and substrate flux increased over the first 15 days of continuous growth; NH_4^+ flux was measured for *N. europaea* biofilms; glucose flux was measured for *P. aeruginosa* biofilms (Fig. 1, panels C and D), and did not significantly change after approximately 3 weeks of growth at $Re = 20$ ($P = 7.3 \times 10^{-6}$, $\alpha = 0.05$). Based on the steady state parameters defined by McLamore et al. (2009, 2010a), oxygen and substrate flux were at steady state after 3 weeks. No significant difference between oxygen and

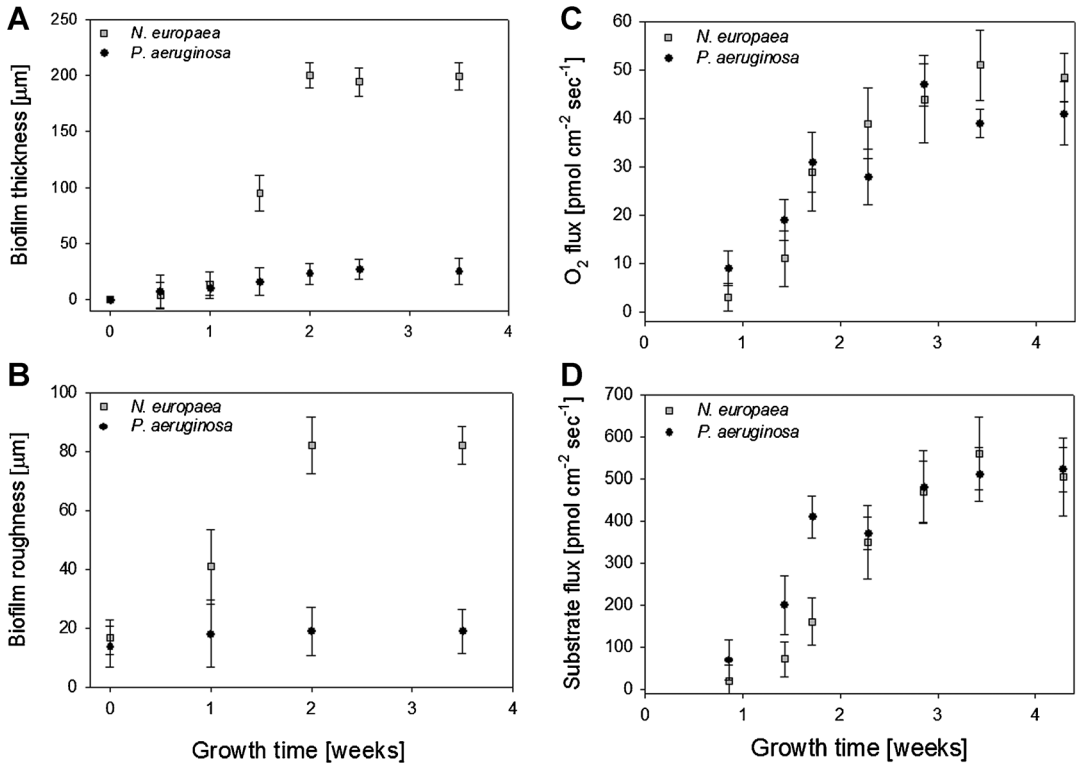

Figure 1. Physiology (form and function) during development of monoculture *N. europaea* and *P. aeruginosa* biofilms grown on PDMS fibers at a mean stream velocity of 23 mm s^{-1} ($Re = 20$) in upflow HfMBR. **Panels A and B**: Average thickness and roughness for biofilms ($n = 6$) grown in flowcells at $Re = 20$. **C**: Average oxygen flux along the surface of biofilms during development. **D**: Average substrate flux along the surface of *N. euopaea* and *P. aeruginosa* biofilms (NH_4^+ flux for *N. europaea* and glucose flux for *P. aeruginosa).* All error bars represent standard error of the arithmetic mean ($n = 6$).

substrate flux was observed for *N. europaea* and *P. aeruginosa* biofilms. The steady state flux values measured for mature *N. europaea* and *P. aeruginosa* were not significantly different than previous values reported in the literature for HfMBR biofilms operated at $Re = 35$ (McLamore et al., 2009, 2010a; Jaroch et al., 2011). The observed steady state metabolism, surface roughness and thickness after approximately 3 weeks at $Re = 20$ indicate that *N. euroopaea* and *P. aeruginosa* biofilms reached steady state growth. For thin biofilms on gas-permeable membranes (such as *P. aeruginosa* in these experiments), oxygen flux from the membrane lumen can diffuse into the bulk liquid, and measurement of microprofiles using traditional microelectrodes may not account for this experimental bias. The SR fiber optic sensors used in these studies can monitor oxygen flux from the bulk liquid into the biofilm. This is a major technical advantage that allows direct measurement of the metabolic oxygen uptake along the surface of the biofilm (McLamore et al., 2010a,b).

Poplawski et al. (2008) proposed that biofilm morphology depends on the non-dimensional ratio (R) of the maximum biomass growth rate to the maximum substrate transport rate. In their studies, biofilm growth was either growth rate limited (high R values) or nutrient transport limited (low R values). When the growth rate is limiting, substrate is easily transported and will penetrate most of the biofilm. These biofilms tend to be flat, compact and fast-growing. When transport limits growth, the substrate penetrates only the top thin layers of the biofilm. In this growth state, Poplawski et al. (2008) concluded that cells tend to protrude out of the biofilm, and biofilm roughness is significantly higher than growth limited biofilms; the higher surface area increases mass transport of nutrients. Other researchers have noted that transport limited biofilms with a low specific growth rate may have an increased production of EPS, although this is often species specific (Boe-Hansen et al., 2002; Kindaichi et al., 2004, 2006; Okabe et al., 2005; Rittmann et al., 1994). Based on the growth rates estimated using biofilm thickness (Fig. 1A) and the maximum substrate flux (Fig. 1D), the modified R ratio defined by Poplawski et al. (2008) for *N. europaea* (8.5 ± 1.2) was significantly higher than *P. aeruginosa* (0.5 ± 0.3). Based on these calculated ratios, *N. europaea* biofilms should have a higher roughness than *P. aeruginosa.* This trend was confirmed based on the data in Figure 1B.

To further investigate the rate limiting growth state of the developing biofilms, effluent biomass was measured from the flow cells during development (Fig. 2A). A short lag

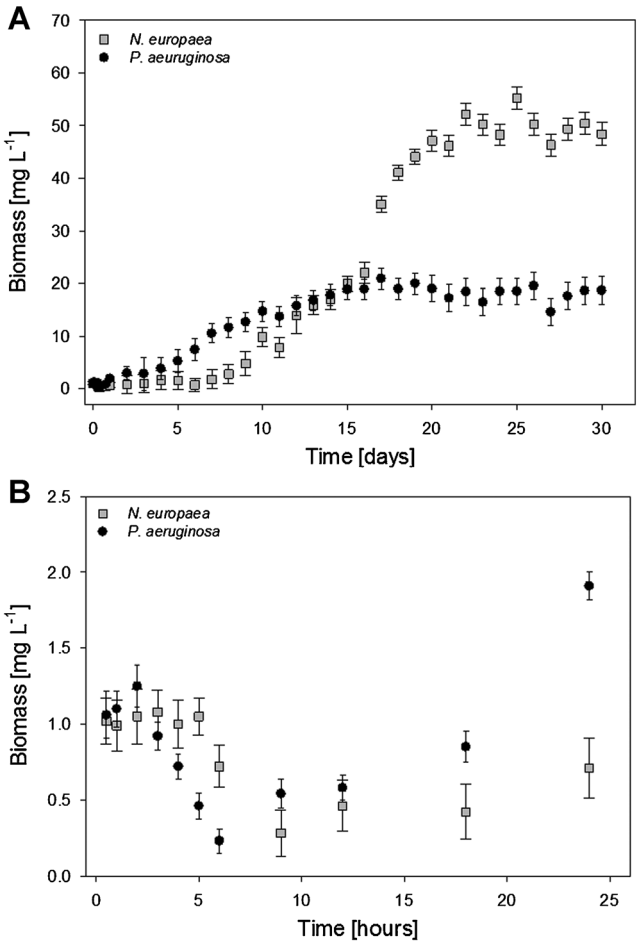

Figure 2. **A**: Effluent biomass from flowcells for *N. europaea* and *P. aerugionsa* biofilms grown at $Re = 20$ (23 mm s^{-1}) for 30 days ($n = 6$). **B**: Exploded view of the first 24 h of biomass development from panel A.

phase in effluent biomass was measured for both species, followed by steady state behavior after 21–24 days for both biofilms. The observed exponential response in Figure 2A is similar to trends observed in the literature and stochastic detachment models (Bohn et al., 2007; Picioreanu et al., 2000; Stoodley et al., 2001, 2002b; Xavier et al., 2005). The lag phase for *P. aeruginosa* (2–3 days) was shorter than *N. europaea* (5–6 days); lag time was defined as less than a 5% change in effluent biomass. During the first 10–12 days, *P. aeruginosa* growth rate was higher than *N. europaea* biofilms (i.e., lower effluent biomass 3–6; Fig. 2B). Interestingly, after 12–14 days, the biomass measured in the *P. aeuruginosa* flowcell effluent (17.8 ± 1.4 mg-biomass L^{-1}) was significantly lower than *N. europaea* effluent biomass (49.7 ± 2.7 mg-biomass L^{-1}). This difference in biomass was likely due to the increased thickness of *N. europaea* biofilms relative to *P. aeruginosa* (Fig. 1A), and may also be related to relatively high roughness of *N. europaea* biofilms after 2 weeks of growth. To investigate possible correlations between detachment, thickness, roughness, and species type, detailed shear-induced detachment studies were conducted using mature biofilms.

During microcolony formation planktonic cells are undergoing reversible attachment, cohesion, or coaggregation as planktonic cells begin to undergo physiological changes and produce a dense exopolymeric matrix. Thus, one would expect the passive (i.e., externally driven) detachment rate to be relatively high during this growth phase. In natural systems (e.g., rivers) where the number of cells entering a control volume is dynamic, the detachment rate for a mature biofilm is approximately equal to the attachment rate under steady state conditions (Kwok et al., 1998; Xavier et al., 2005). However, in a closed microbial system such as a bioreactor under constant loading, no cells are continuously entering the system, and the detachment rate is equal to the growth rate under steady state conditions.

Surface Shear Stress

To estimate the effect of fluid shear on biofilm detachment, microscale velocity profiles were measured near the surface of mature biofilms for three different flow rates (5, 10, and 15 mL/min) using a μ-PIV (all biofilms were developed and transferred to flowcells as previously described). The measured velocity profiles followed predicted behavior based on boundary layer momentum transport theory. As expected, the measured velocity near all biofilm surfaces was approximately zero (due to the no-slip condition at the biofilm–liquid interface) and velocity exponentially increased with distance from the biofilm surface (Fig. 3A). Surface shear stress (defined as the force at the biofilm surface caused by hydrodynamic drag) was calculated using Equation (1) and the measured linear portion of the velocity–distance plots (du/dy) in Figure 3A. A representative plot of calculated du/dy values for a mature *N. europaea* biofilm is shown in Figure 3B. Velocity profiles above all biofilms and RMS values may be found in the Supplementary Section (Fig. S2). Linear regression for all du/dy plots had an R^2 value >0.98.

Hydrodynamic boundary layer (HBL) thickness was calculated at various fluid velocities using μ-PIV velocity profiles. Biofilm roughness for mature biofilms ranged from 350 to 595 μm (recall Fig. 1B). HBL thickness decreased with increasing free stream velocity, which is consistent with expected trends for momentum transport describing compressed HBL under increasing fluid shear (Picioreanu et al., 2000) (Fig. 4A). Relatively thin biofilms (e.g., 1-week-old *P. aeruginosa* biofilms) had an average HBL thickness which was not statistically different than a clean (sterile) membrane ($P = 4.3 \times 10^{-4}$, $\alpha = 0.05$). All other biofilms (i.e., mature *P. aeruginosa* and all *N. europaea* biofilms) had an HBL thickness that was significantly greater than sterile PDMS fibers ($P = 1.5 \times 10^{-6}$, $\alpha = 0.05$). HBL thickness for

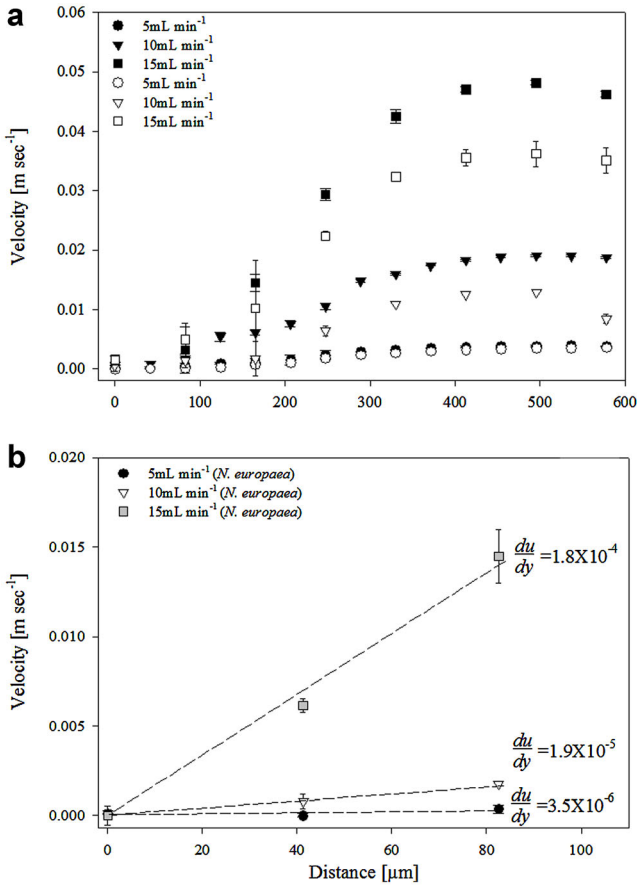

Figure 3. Representative velocity profile above the surface of a *N. europaea* biofilm at various flowrates measured via μ-PIV. **Panel a**: Open symbols represent average values for biofilms after 10 days of continuous growth; closed symbols represent average values for biofilms after 3 weeks of continuous growth. **Panel b**: The particle velocity within the linear portion of the hydrodynamic boundary layer was used to estimate the shear stress at the biofilm surface (3-week-old *N. europaea* biofilm shown).

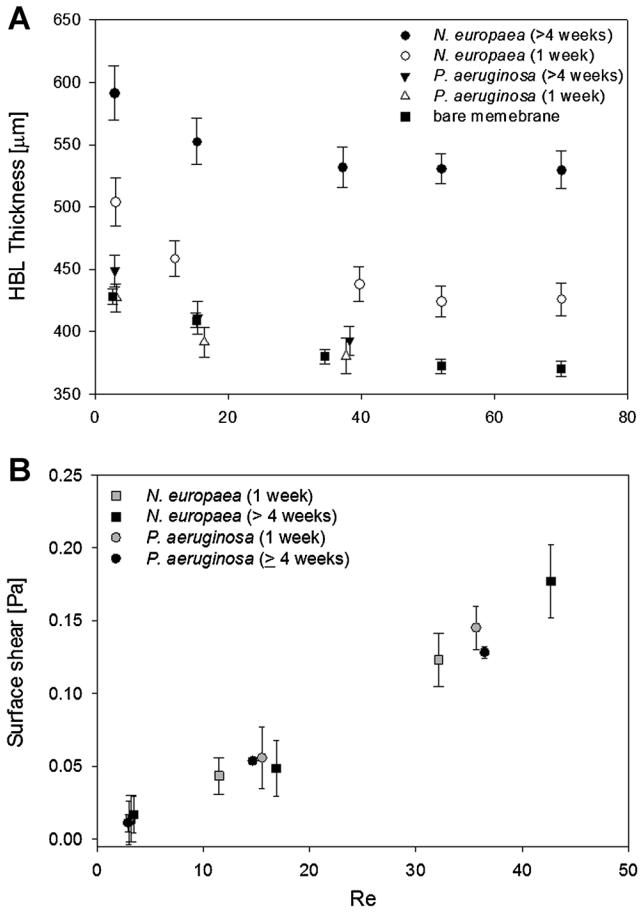

Figure 4. **A**: Hydrodynamic boundary layer (HBL) thickness measured at the biofilm surface as a function of mean stream velocity. A bare membrane is shown for comparison purposes (■). HBL thickness was calculated as the location where the measured velocity (via μ-PIV) was 99% of mean stream velocity Error bars represent standard error of the arithmetic mean ($n = 3$). **B**: Calculated shear for all biofilms a function of fluid flow (shown as axial Reynolds number).

N. europaea biofilms was significantly larger than *P. aeruginosa* biofilms. The largest HBL values were observed for mature *N. europaea*, which had the highest surface roughness (82 ± 8 μm), followed by microcolony *N. europaea* (60 ± 3 μm).

Using the measured d*u*/d*y* values and Equation (1), surface shear was calculated for *Re* values between 1 and 40 for *N. europaea* and *P. aeruginosa* biofilms (both 1-week-old and mature biofilms ≥4 weeks old were measured). As expected, increased mean stream velocity resulted in an increase in surface shear stress for all biofilms. For both species of biofilm, there was no significant difference between the measured shear stress for 3-week-old and 1-week-old biofilms ($P = 5.0 \times 10^{-3}$, $\alpha = 0.05$). However, the measured average shear stress at the surface of *N. europaea* biofilms (54.5 ± 3.2 mPa) was approximately 20% larger than the shear for *P. aeruginosa* biofilms (45.8 ± 7.7 mPa).

Passive Detachment

In preliminary experiments using mature biofilms, biomass was measured following transfer of samples from HfMBR to ensure sampling did not cause significant detachment. After transfer to the flowcell, the samples were allowed to equilibrate to new conditions for 1 h, liquid was removed, and biomass was measured. For six replicate biofilms, detachment due to sample transfer was near the lower limit of detection for the coulter counter (*N. europaea* was 0.22 mg-biomass L^{-1}; *P. aeruginosa* was 0.13 mg-biomass L^{-1}).

For all biofilms measured (conditions between $Re = 10$–60), detachment from *N. europaea* biofilms was significantly higher than detachment from *P. aeruginosa* biofilms (approximately $37 \pm 18\%$ higher for all samples tested; Fig. 5). Detachment of mature biofilms (≥4 weeks) was significantly larger than detachment of 1-week-old biofilms

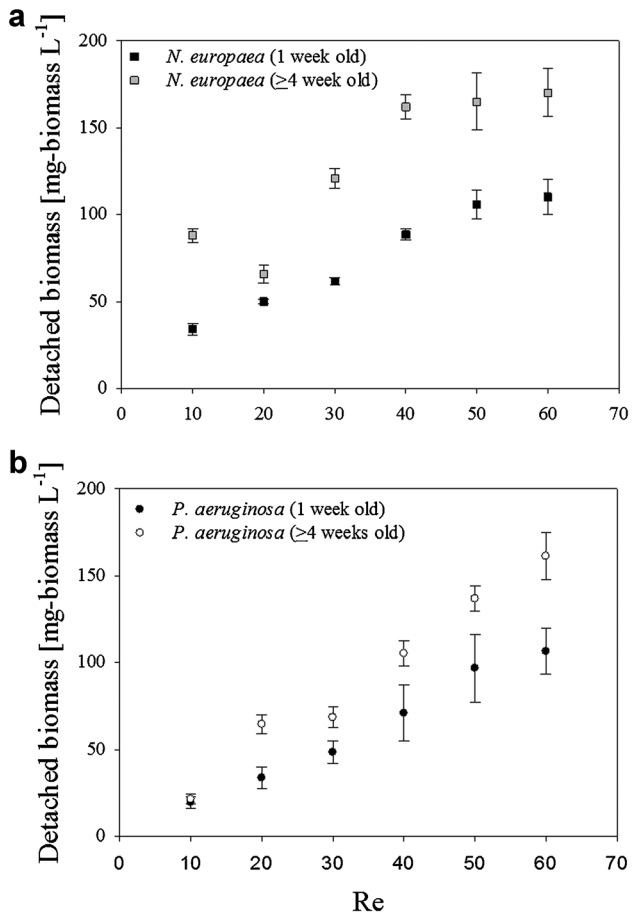

Figure 5. Passive detachment from (**A**) *N. europaea* biofilms and (**B**) *P. aeruginosa* biofilms after 1-week (microcolony) and 4 weeks (mature) of continuous growth. Error bars represent standard deviation ($n = 3$).

($P = 0.9 \times 10^{-2}$, $\alpha = 0.05$). The highest measured detached biomass concentration (170 ± 13 mg-biomass L^{-1}) was measured for mature ($\geq$4 weeks old) *N. europaea* biofilms at $Re = 61$ (69 mm s^{-1}). Detachment of mature *P. aeruginosa* was slightly lower (161 ± 13 mg-biomass L^{-1}), but significantly different. In preliminary experiments, velocities above 85 mm s^{-1} ($Re \approx 75$) caused total detachment of microcolony biofilms and detachment from hollow fibers (data not shown). Interestingly, passive detachment of mature *N. europaea* biofilms was significantly larger than mature *P. aeruginosa* biofilms, especially when *Re* was smaller than 60. This phenomenon was consistent with the fact that the measured average shear stress at the surface of *N. europaea* biofilms was approximately 20% larger than the shear for *P. aeruginosa* biofilms. Another reason may be that *N. europaea* biofilm has a much thicker biofilm and therefore more cells/polymers were able to detach from the surface. Other studies have reported relatively high extracellular polymer (EPS) content in *N. europaea* biofilms (Boe-Hansen et al., 2002; Kindaichi et al., 2004, 2006; Okabe et al., 2005; Rittmann et al., 1994). While the production of EPS is a metabolic burden, it is also a survival mechanism that provides protection from, stressors, predators, and possibly passive detachment (Lim et al., 2011; Purevdorj-Gage et al., 2005). While no significant difference in metabolism (substrate or oxygen flux) was observed, the relatively high roughness of *N. europaea* biofilms increased the overall surface area under the influence of fluid shear. Detailed studies to confirm the link between EPS production and passive detachment are outside the scope of this work, but these studies are needed to understand the correlation between physiology and detachment rate.

Passive biofilm detachment has been studied in a number of engineered bioreactors, including airlift suspension reactors (Kwok et al., 1998), granular sludge reactors (Liu and Tay, 2002), as well as catheters (Fux et al., 2004), glass cover slides and flow cells (Klapper et al., 2002; Stoodley et al., 2002b). Although empirical studies and the development of mathematical models have increased our understanding of the relationship between biofilm formation and mass/momentum boundary layer transport (Eberl et al., 2000; Matsumoto et al., 2007; Xavier et al., 2005), there are minimal published in situ data quantifying transport phenomena in membrane bioreactors. In addition to the unique physiology of HfMBR (i.e., counter diffusion biofilms), fundamental studies such as these improve our basic understanding of biofilm formation on hollow fibers. Wijeyekoon et al. (2000) highlights how subtle difference in geometry can result in relatively large differences in phenotype formation.

Conclusions

A unique set of experimental methods was used to quantify the correlation between biofilm physiology, fluid-induced shear stress, and detachment in hollow fiber membrane aerated bioreactors using two monoculture biofilms. Surface shear stress was demonstrated to be an important parameter in the prediction of passive detachment events. No significant difference was noted when comparing shear stress for immature and mature biofilms of the same species. Surface shear stress was higher for *N. europaea* biofilms (54.5 ± 3.2 mPa) when compared with *P. aeruginosa* biofilms (45.8 ± 7.7 mPa), resulting in higher biofilm detachment. There was a significant difference in detached biomass for immature vs. mature biofilms in both species. However, there was no difference in detachment rate between the two species. Results from this research indicate that the operation of nitrifying HfMBR with mean stream velocities $\approx$23 mm s^{-1} may optimize reactor performance. This information would be particularly applicable during initial biofilm development when detachment rates of nitrifying communities may be considerably higher and may have implications for rapid reactor startup, shock loading, and cell-templated layering of communities in bioreactors.

The authors would like to thank Purdue University for support during this research project.

References

Auerbach ID, Sorensen C, Hansma HG, Holden AH. 2000. Physical morphology and surface properties of unsaturated *Pseudomonas putida* biofilms. J Bacteriol 182(13):3809–3815.

Beyenal H, Chen SN, Lewandowski Z. 2003. The double substrate growth kinetics of *Pseudomonas aeruginosa*. Enzyme Microbial Technol 32: 92–98.

Bishop PL, Gibbs JT, Cunningham BE. 1997. Relationship between concentration and hydrodynamic boundary layers over biofilms. Environ Technol 18:375–385.

Boe-Hansen R, Albrechtsen HJ, Arvin E, Jorgensen C. 2002. Bulk water phase and biofilm growth in drinking water at low nutrient conditions. Water Res 36:4477–4486.

Bohn A, Zippel B, Almeida JS, Xavier JB. 2007. Stochastic modeling for characterisation of biofilm development with discrete detachment events (sloughing). Water Sci Technol 55(8–9):257–264.

Boles BR, Thoendel M, Singh PK. 2005. Rhamnolipids mediate detachment of *Pseudomonas aeruginosa* from biofilms. Mol Microbiol 57:1210–1223.

Casey E, Glennon B, Hamer G. 1999. Oxygen mass transfer characteristics in a membrane-aerated reactor. Biotechnol Bioeng 62:183–192.

Casey E, Glennon B, Hamer G. 2000. Biofilm development in a membrane-aerated biofilm reactor: Effect of flow velocity on performance. Biotechnol Bioeng 67:476–486.

Chen MJ, Zhang Z, Bott TR. 1998. Direct measurement of the adhesive strength of biofilms in pipes by micromanipulation. Biotechnol Tech 12:875–880.

Cole SP, Hardwood J, Lee R, She R, Guiney DG. 2004. Characterization of monospecies biofilm formation by *Helicobacter pylori*. J Bacteriol 186:3124–3132.

Cote P, Bersillion JL, Huyard A. 1989. Bubble-free aeration using membranes: Mass transfer analysis. J Membr Sci 47:91–106.

Eberl HJ, Picioreanu C, Heijnen JJ, van Loosdrecht MCM. 2000. A three-dimensional numerical study on the correlation of spatial structure, hydrodynamic conditions, and mass transfer and conversion in biofilms. Chem Eng Sci 55:6209–6222.

EPA. 2001. Method 1684: Total, Fixed, and Volatile Solids in Water, Solids and Biosolids. US. Environmental Protection Agency Office of Water, Office of Science and Technology, Engineering and Analysis Division (4303); EPA-821-R-01-015.

Fux CA, Wilson S, Stoodley P. 2004. Dispersal characteristics and antimicrobial susceptibility to emboli from *Staphylococcus aureus* biofilms in an *in-vitro* catheter infection model. J Bacteriol 186:4486–4491.

Hibiya K, Terada A, Tsuneda S, Hirata A. 2003. Simultaneous nitrification and denitrification by controlling vertical and horizontal microenvironment in a membrane-aerated biofilm reactor. J Biotechnol 100: 23–32.

Higuchi H, Sawada H, van Langen P. 2005. Flow over a magnetically suspended cylinder in an axial free stream. PROC AIAA 1078:1–10.

Jaroch D, McLamore ES, Zhang W, Shi J, Garland JL, Banks MK, Porterfield DM, Rickus JL. 2011. Cell-mediated silica entrapment of bacterial biofilms. Biotechnol Bioeng 108:2249–2260.

Kindaichi T, Kawano Y, Ito T, Satoh H, Okabe S. 2006. Population dynamics and in situ kinetics of nitrifying bacteria in autotrophic nitrifying biofilms as determined by real-time quantitative PCR. Biotechnol Bioeng 94:1111–1121.

Kindaichi T, Okabe S, Satoh H, Watanabe Y. 2004. Effects of hydroxylamine on microbial community structure and function of autotrophic nitrifying biofilms determined by in situ hybridization and the use of microelectrodes. Water Sci Technol 49:61–68.

Klapper I, Rupp CJ, Cargo R, Purevdorj B, Stoodley P. 2002. A viscoelastic fluid description of bacterial biofilm material properties. Biotechnol Bioeng 80:289–296.

Kwok WK, Picioreanu C, Ong SL, van Loosdrecht MCM, Ng WJ, Heijnen JJ. 1998. Influence of biomass production and detachment force on biofilm structures in a biofilm airlift suspension reactor. Biotechnol Bioeng 58:400–407.

Li T, Bai R, Ohandja D, Liu J. 2009. Biodegradation of acetonitrile by adapted biofilm in a membrane-aerated biofilm reactor. Biodegradation 20:569–580.

Lim J, Cui Y, Oh YJ, Park JR, Jo W, Cho YH, Park S. 2011. Studying the effect of alginate overproduction on *Pseudomonas aeruginosa* biofilm by atomic force microscopy. J Nanosci Nanotechnol 11:5676–5681.

Liu Y, Tay J. 2002. The essential role of hydrodynamic shear force in the formation of biofilm and granular sludge. Water Res 36:1653–1665.

Matsumoto S, Terada A, Aoi Y, Tsuneda S, Alpkvist E, Picioreanu C, van Loosdrecht MCM. 2007. Experimental and simulation analysis of communitystructure of nitrifying bacteria in a membrane-aerated biofilm. Water Sci Technol 55:283–290.

McLamore ES, Jackson WA, Morse A. 2007. Abiotic transport in a membrane aerated bioreactor. J Membr Sci 298:110–116.

McLamore ES, Porterfield DM, Banks MK. 2009. Non-invasive self-referencing electrochemical sensors for quantifying real time biofilm analyte flux. Biotechnol Bioeng 102:791–799.

McLamore ES, Zhang W, Porterfield DM, Banks MK. 2010a. Membrane-aerated biofilm proton and oxygen flux during chemical toxin exposure. Environ Technol 44:7050–7057.

McLamore ES, Stensberg M, Yale M, Ochoa-Acuna H, Sepulveda M, Sun X, Akkus O, Porterfield DM. 2010b. An optical imaging technique for monitoring real time changes in morphology within the cell, tissue, or whole organism spatial domain. Proceedings of SPIE-International Society of Optical Engineering. Paper No. 7674-14.

McLamore ES, Porterfield DM. 2011. Non-invasive tools for measuring metabolism and biophysical analyte transport: Self-referencing physiological sensing. Chem Soc Rev 40:5308–5320.

McLamore ES, Shi J, Jaroch D, Barcus C, Osbourne J, Uchida A, Jiang Y, Buhman KK, Banks MK, Teegarden D, Rickus JL, Porterfield DM. 2011. A self referencing enzyme-based microbiosensor for real time measurement of physiological glucose transport. Biosens Bioelectron 26:2237–2245.

Ohashi A, Harada H. 1994. Adhesion strength of biofilm developed in an attached-growth reactor. Water Sci Technol 29:10–11.

Okabe S, Kindaichi T, Ito T. 2005. Fate of 14C-labeled microbial products derived from nitrifying bacteria in autotrophic nitrifying biofilms. Appl Environ Microbiol 71:3987–3994.

Pankhania M, Stephenson T, Semmens MJ. 1994. Hollow fibre bioreactor for wastewater treatment using bubbleless membrane aeration. Water Res 28:2233–2236.

Picioreanu C, van Loosdrecht MCM, Heijnen JJ. 1998. Mathematical modeling of biofilm structure with a hybrid differential-discrete cellular automaton approach. Biotechnol Bioeng 58:101–116.

Picioreanu C, van Loosdrecht MCM, Heijnen JJ. 2000. A theoretical study on the effect of surface roughness on mass transport and transformation in biofilms. Biotechnol Bioeng 68:355–369.

Picioreanu C, van Loosdrecht MCM, Heijnen JJ. 2001. Two-dimensional model of biofilm detachment caused by internal stress. Biotechnol Bioeng 7:205–218.

Purevdorj-Gage B, Costerton WJ, Stoodley P. 2005. Phenotypic differentiation and seeding dispersal in non-mucoid and mucoid *Pseudomonas aeruginosa* biofilms. Microbiology 151:1569–1576.

Poplawski NJ, Shirinifard A, Swat M, Glazier JA. 2008. Simulation of single-species bacteria-biofilm growth using the Glazier-Graner-Hogeweg model and the compucell3d modeling environment. Math Biosci Eng 5:355–388.

Prosser JI. 1989. Autotrophic nitrification in bacteria. Adv Microb Physiol 30:125–181.

Rector TJ, Garland JL, Starr SO. 2006. Dispersion characteristics of a rotating hollow fiber membrane bioreactor: Effects of module packing density and rotational frequency. J Membr Sci 278:144–150.

Rittmann BE, Regan JM, Stahl DA. 1994. Nitrification as a source of soluble organic substrate in biological treatment. Water Sci Technol 30:1–8.

Sahinkaya E, Hasar H, Kaksonen AH, Rittmann BE. 2011. Performance of a sulfide-oxidizing, sulfur-producing membrane biofilm reactor treating sulfide-containing bioreactor effluent. Environ Sci Technol 45:4080–4087.

Santiago JG, Wereley ST, Meinhart CD, Beebe DJ, Adrian RJ. 1998. A particle image velocimetry system for microfluidics. Exp Fluids 25: 316–319.

Shanahan J, Semmens MJ. 2007. Characterization studies of nitrifying biofilms growing on gas-permeable, flat sheet membranes. 4th IWA Conference on membranes for water and wastewater treatment 15–17. Harrogate, United Kingdom.

Stoodley P, Hall-Stoodley L, Lappin-Scott HM. 2001. Detachment, surface migration, and other dynamic behavior in bacterial biofilms revealed by digital time-lapse imaging. Method Enzymol 337:306–319.

Stoodley P, Sauer K, Davies DG, Costerton JW. 2002a. Biofilms as complex differentiated communities. Annu Rev Microbiol 56:187–209.

Stoodley P, Cargo R, Rupp CJ, Wilson S, Klapper I. 2002b. Biofilm material properties as related to shear-induced deformation and detachment phenomena. J Ind Microbiol Biotechnol 29:361–368.

Stoodley LH, Costerson JW, Stoodley P. 2004. Bacterial biofilms: From the natural environment to infectious disease. Nat Rev Microbiol 2: 95–108.

Stoodley P, Dodds I, De Beer D, Scott HL, Boyle JD. 2005. Flowing biofilms as a transport mechanism for biomass through porous media under laminar and turbulent conditions in a laboratory reactor system. Biofouling 21:161–168.

Suzuki Y, Hatano N, Ikeda H. 2000. Performance of nitrogen removal and biofilm structure of porous gas permeable membrane reactor. Water Sci Technol 41(4–5):211–217.

Tansel B, Sager J, Rector T, Garland J, Strayer RF, Levine L, Roberts M, Hummerick M, Bauer J. 2005. Integrated evaluation of a sequential membrane filtration system for recovery of bioreactor effluent during long space missions. J Membr Sci 255:117–124.

Tansel B, Sager J, Garland J, Xu S, Levine L, Bisbee P. 2006. Deposition of extracellular polymeric substances (EPS) and microtopographical changes on membrane surfaces during intermittent filtration conditions. J Membr Sci 285:225–231.

Terada A, Hibiya K, Nagai J, Tsuneda S, Hirata A. 2003. Nitrogen removal characteristics and biofilm analysis of a membrane-aerated biofilm reactor applicable to high-strength nitrogenous wastewater treatment. J Biosci Bioeng 95:170–178.

van Loosdrecht MCM, Eikelboom D, Gjaltema A, Mulder A, Tijhuis L, Heijnen JJ. 1995. Biofilm structures. Water Sci Technol 32:35–43.

Wang R, Terada A, Lackner S, Steets BF, Henze M, Xia S, Zhao J. 2009. Nitritation performance and biofilm development of co and counter-diffusion biofilm reactors: Modeling and experimental comparison. Water Res 43(10):2699–2709.

Wijeyekoon S, Mino T, Satoh H, Matsuo T. 2000. Growth and novel structural features of tubular biofilms produced under different hydrodynamic conditions. Water Sci Technol 41:129–138.

Wimpenny JWT, Colasanti R. 1997. A unifying hypothesis for the structure of microbial biofilms based on cellular automaton models. FEMS Microbiol Ecol 22:1–16.

Xavier JD, Picioreanu C, van Loosdrecht MCM. 2005. A general description of detachment for multidimensional modelling of biofilms. Biotechnol Bioeng 91:651–669.

Yamagiwa K, Yoshida M, Akira I, Ohkawa A. 1998. A new oxygen supply method for simultaneous organic carbon removal and nitrification by a one-stage biofilm process. Water Sci Technol 37:117–124.